


Structure changes along the lowest rotational band of the antiprotonic helium atom

Daniel Baye,^{*} Jérémy Dohet-Eraly,[†] and Philippe Schoofs[‡]
*Physique Quantique, and Physique Nucléaire Théorique et Physique Mathématique,
 C.P. 229, Université libre de Bruxelles (ULB), B-1050 Brussels, Belgium*

 (Received 14 November 2018; published 21 February 2019)

Along its lowest rotational band, the antiprotonic helium atom undergoes several changes of structure. It evolves from an hydrogenlike atom with broader and broader resonant states, to a quasistable molecularlike structure with narrow resonances, and then to a quasistable Rydberg pseudoatom. The antiprotonic helium atom is studied with high accuracy as a nonrelativistic three-body Coulomb system in the framework of the Lagrange-mesh method. Its metastable states are first determined from $L = 0$ to $L = 80$ by searching conditions of calculation for which energies are stationary. Mean values of distances between the particles are then easily deduced. They show the evolution of the structure of the system. Broad resonances are also analyzed with the complex scaling method. Physical interpretations are provided.

DOI: [10.1103/PhysRevA.99.022508](https://doi.org/10.1103/PhysRevA.99.022508)

I. INTRODUCTION

Antiprotonic helium atoms, i.e., systems composed of a helium nucleus, an antiproton, and an electron ($\bar{p}\text{He}^+$), appear when antiprotons are stopped in helium. Their existence was anticipated by the fact that the average annihilation time of the antiproton was anomalously long (see Ref. [1] for a review). As suggested by Condo [2] for mesonic atoms, the antiproton can be captured in states with a large total orbital quantum number L where it replaces a $1s$ electron. These states have long lifetimes because the Auger electron emission is then a slow process. Hence the antiproton annihilation which requires a number of deexcitations of the system is delayed. These ideas were confirmed by calculations of Russell [3–5]. The spontaneous emission of an electron (or autoionization, or Auger decay) is strongly hindered in these orbitals because the electron can be emitted only with a rather high orbital momentum l [3]. Also, in these high excited states with large L values, radiative decays are quite slow. The experimental confirmation of the existence of antiprotonic helium came 20 years later [1,6].

The interest in the antiprotonic helium atom is high since its experimental study opened a way to accurately measure the antiproton mass [1,7,8]. The attempts to deduce antiproton properties from the experimental study of antiprotonic helium required more and more accurate calculations of energies and wave functions [3,7–16]. They were complemented by the evaluation of relativistic and QED corrections [8,11,12,17–19]. Estimating the widths of the observed states was also important. The calculations of Auger widths were in general based on the golden rule [5,9,20], but more elaborate frameworks can also be found [8,20,21]. Radiative decay widths were also determined [1,5,12,22,23].

A series of experiments accurately measuring transitions in the spectrum of antiprotonic helium for total orbital momenta around $L = 35$ [1,24,25] combined with the accurate calculations of three-body energy differences with relativistic and QED corrections allowed researchers to provide the best values of the antiproton mass. Within the present experimental and theoretical error bars, the obtained mass does not differ from the proton mass.

Because of the interest for the antiproton mass, most studies of antiprotonic helium concentrate on high orbital angular momenta, for which this system is most likely to form when antiprotons are stopped in helium. Indeed, except for $L = 0$ [26], the system has been studied only from $L = 28$ up to $L = 41$ mostly by Korobov and coworkers [7,10,11,14,18–20] and by the Kyushu group [8,13,15,17]. Antiprotonic helium, however, is an interesting physical system by itself. It presents a variety of structures and properties along its lowest rotational band, sometimes like an atom, sometimes like a molecule. For this reason, it is also called an atom-molecule or atomcule [1]. The aim of the present work is to complement the knowledge of $\bar{p}\text{He}^+$ by analyzing some of its physical properties from $L = 0$ up to very high L values.

To this end, we treat the $\text{He}^{2+} + \bar{p} + e$ system as a nonrelativistic three-body Coulomb system. Except for the ground state and its electronic excitations, all $\bar{p}\text{He}^+$ states are unstable, though often metastable with very narrow widths. We calculate energies and some geometrical properties in the perimetric coordinate system [27,28] with the help of the Lagrange-mesh method [29–34]. This method has the accuracy of a variational calculation and the simplicity of a mesh calculation. It does not require analytical evaluations of integrals, and computer times are short once optimal sets of parameters are established.

The Lagrange-mesh method offers very accurate results when the states are quasibound, i.e., when the electron emission width is small. When this is not the case, the method can be combined with complex scaling [35,36]. However, the perimetric coordinate system is not favorable for rather broad

^{*}dbaye@ulb.ac.be

[†]jdoheter@ulb.ac.be

[‡]Presently, independent researcher.

resonances, which limits its applicability with the complex-scaling method.

The Lagrange-mesh method is summarized in Sec. II. The conditions of the numerical calculations and various results are presented in Sec. III. They are discussed along the rotational band in Sec. IV. Section V contains a summary and a conclusion. Atomic units (a.u.) are used throughout.

II. THE LAGRANGE-MESH METHOD

We study the lowest rotational band of the three-body system formed by a ${}^4\text{He}^{2+}$ nucleus or α particle of mass $m_\alpha = 7294.299508$, an antiproton of mass $m_{\bar{p}} = 1836.1526675$, and an electron of mass $m_e = 1$. We adopt here the values used in Ref. [8] for the sake of comparison. The particles interact only through the Coulomb force. Fine-structure and relativistic effects are not taken into account.

The Lagrange-mesh method combines a three-dimensional mesh, a basis of Lagrange functions which vanish at all mesh point but one to which they are associated, and a Gauss quadrature consistent with the mesh [29,34]. The Schrödinger equation is solved in perimetric coordinates to avoid problems with the singularities of the kinetic-energy operator and of the Coulomb interactions. The system of perimetric coordinates [27,28] is defined by the three Euler angles ψ, θ, ϕ and the three coordinates

$$\begin{aligned} x &= r_{\alpha\bar{p}} + r_{\alpha e} - r_{\bar{p}e}, \\ y &= r_{\alpha\bar{p}} - r_{\alpha e} + r_{\bar{p}e}, \\ z &= -r_{\alpha\bar{p}} + r_{\alpha e} + r_{\bar{p}e}. \end{aligned} \quad (1)$$

The coordinates x, y , and z vary over the $(0, \infty)$ interval. The volume element reads [32,37]

$$dV = (x+y)(y+z)(z+x) \sin\theta \, d\psi \, d\theta \, d\phi \, dx \, dy \, dz. \quad (2)$$

In perimetric coordinates, the Coulomb potential reads

$$V(x, y, z) = -\frac{4}{x+y} - \frac{4}{x+z} + \frac{2}{y+z}. \quad (3)$$

The kinetic energy operator for S states is given, e.g., in Ref. [38]. The general expression for arbitrary states can be found in Ref. [33].

The wave function with total orbital momentum L and natural parity $(-1)^L$ is expanded as [33]

$$\Psi_M^L = \sum_{K=0}^L \mathcal{D}_{MK}^L(\psi, \theta, \phi) \Phi_K^L(x, y, z). \quad (4)$$

In some cases, for $L > 0$, the sum can be truncated with excellent accuracy at some value K_{\max} . The normalized angular functions $\mathcal{D}_{MK}^L(\psi, \theta, \phi)$ are defined for $K \geq 0$ by

$$\begin{aligned} \mathcal{D}_{MK}^L(\psi, \theta, \phi) &= \frac{\sqrt{2L+1}}{4\pi} (1 + \delta_{K0})^{-1/2} [\mathcal{D}_{MK}^L(\psi, \theta, \phi) \\ &+ (-1)^K \mathcal{D}_{M-K}^L(\psi, \theta, \phi)], \end{aligned} \quad (5)$$

where $\mathcal{D}_{MK}^L(\psi, \theta, \phi)$ represents a Wigner matrix element.

Now let us define the Lagrange basis. Let u_i, v_j, w_k be the zeros of Laguerre polynomials of respective degrees N_x, N_y, N_z , and h_x, h_y, h_z be three scale parameters with the dimension of a length. The Lagrange function associated with

the three-dimensional mesh point $(h_x u_i, h_y v_j, h_z w_k)$ is defined as

$$\begin{aligned} F_{ijk}^K(x, y, z) &= \mathcal{N}_{Kijk}^{-1/2} \mathcal{R}_K(x, y, z) f_i^{(N_x)}(x/h_x) \\ &\times f_j^{(N_y)}(y/h_y) f_k^{(N_z)}(z/h_z), \end{aligned} \quad (6)$$

where

$$f_n^{(N)}(u) = (-1)^n u_n^{1/2} \frac{L_N(u)}{u - u_n} e^{-u/2} \quad (7)$$

is a one-dimensional Lagrange-Laguerre function, $L_N(u)$ is a Laguerre polynomial, and u_n is one of its zeros. The function $\mathcal{R}_K(x, y, z)$ is a regularization factor introduced because of the presence of singularities in the kinetic-energy part of the Hamiltonian operator when L differs from zero (see Refs. [33,37] for details). It is equal to 1 when $K = 0$ and to $\sqrt{xyz(x+y+z)}$ otherwise. The normalization factor \mathcal{N}_{Kijk} is defined as

$$\begin{aligned} \mathcal{N}_{Kijk} &= h_x h_y h_z (h_x u_i + h_y v_j) (h_x u_i + h_z w_k) \\ &\times (h_y v_j + h_z w_k) \mathcal{R}_{Kijk}^2, \end{aligned} \quad (8)$$

where $\mathcal{R}_{Kijk} = \mathcal{R}_K(h_x u_i, h_y v_j, h_z w_k)$. The Lagrange functions verify the Lagrange conditions

$$\begin{aligned} F_{ijk}^K(h_x u_{i'}, h_y v_{j'}, h_z w_{k'}) &= (\lambda_i \mu_j \nu_k \mathcal{N}_{Kijk})^{-1/2} \\ &\times \mathcal{R}_{Kijk} \delta_{i'i} \delta_{j'j} \delta_{k'k}, \end{aligned} \quad (9)$$

i.e., $F_{ijk}^K(x, y, z)$ vanishes at all mesh points except at the ijk point. A triple Gauss-Laguerre quadrature with weights $\lambda_i \mu_j \nu_k$ is associated with this mesh,

$$\begin{aligned} \int_0^\infty \int_0^\infty \int_0^\infty G(x, y, z) \, dx \, dy \, dz &\approx h_x h_y h_z \sum_{i=1}^{N_x} \lambda_i \\ &\times \sum_{j=1}^{N_y} \mu_j \sum_{k=1}^{N_z} \nu_k G(h_x u_i, h_y v_j, h_z w_k), \end{aligned} \quad (10)$$

with which all matrix elements are computed. At the Gauss quadrature approximation, the functions F_{ijk}^K are orthonormal for fixed K . More generally, matrix elements of an operator $O(x, y, z)$ which does not include derivatives are diagonal and given by the values of the operator at the three-dimensional mesh points because of the Lagrange property (9),

$$\begin{aligned} \langle F_{ijk}^K | O(x, y, z) | F_{i'j'k'}^K \rangle_G &= O(h_x u_i, h_y v_j, h_z w_k) \delta_{i'i} \delta_{j'j} \delta_{k'k}, \end{aligned} \quad (11)$$

where the subscript G indicates that the integrals are approximated with Gauss quadratures. This is the case for the potential part of the Schrödinger equation.

The Lagrange-mesh method can be very accurate. It is almost as accurate as a variational calculation with the same basis [31,34]. Strangely, its accuracy for the lowest energies is much better than the accuracy of the Gauss quadrature for individual matrix elements. The Gauss quadrature can lose its accuracy when integrands present singularities or discontinuities, and the Lagrange-mesh method then also becomes inaccurate. This problem is solved when the singularities are regularized [30,34,39], i.e., when multiplicative factors render the integrands nonsingular.

The potential is regularized by the volume element, i.e., the corresponding operator $O(x, y, z)$ in Eq. (11) is the nonsingular product of $V(x, y, z)$ and the Jacobian part in Eq. (2). The kinetic matrix elements are also automatically regularized by the volume element and by $\mathcal{R}_K(x, y, z)$ (see Refs. [32,33,37] for details), i.e., no singular term appears when these matrix elements are calculated with a Gauss quadrature.

The $\Phi_K^L(x, y, z)$ functions in Eq. (4) are expanded in the Lagrange basis as

$$\Phi_K^L(x, y, z) = \sum_{i=1}^{N_x} \sum_{j=1}^{N_y} \sum_{k=1}^{N_z} C_{Kijk}^L F_{ijk}^K(x, y, z). \quad (12)$$

The variational calculation then reduces to the system of $N_x N_y N_z$ mesh equations

$$\sum_{Kijk} \left\{ \langle F_{i'j'k'}^{K'} | T_{K'K}^L | F_{ijk}^K \rangle_G + [V(h_x u_i, h_y v_j, h_z w_k) - E] \delta_{KK'} \delta_{i'i'} \delta_{j'j'} \delta_{kk'} \right\} C_{Kijk}^L = 0, \quad (13)$$

where $T_{K'K}^L$ is the matrix element of the kinetic-energy operator between functions $\mathcal{D}_{MK'}^L$ and \mathcal{D}_{MK}^L . The integration over the angular coordinates is treated analytically, and the integrations over the dimensioned perimetric coordinates are performed with the Gauss-Laguerre quadrature associated with the Lagrange mesh as indicated by the subscript G and by the simplicity of the diagonal potential term. The expression of the kinetic-energy part calculated with this three-dimensional Gauss quadrature is rather long but not very complicated to compute. It is given in the appendix of Ref. [33]. It involves only Laguerre zeros and weights, also appearing in values of the first derivatives of the Lagrange functions at mesh points. Note that the resulting Hamiltonian matrix is sparse.

The wave functions are normed at the Gauss approximation according to

$$\sum_{Kijk} (C_{Kijk}^L)^2 = 1. \quad (14)$$

Several mean values are easily obtained at the Gauss approximation. For example, the mean distance between the helium nucleus and the antiproton is given by

$$\langle r_{\alpha\bar{p}} \rangle_G = \frac{1}{2} \sum_{Kijk} (C_{Kijk}^L)^2 (h_x u_i + h_y v_j). \quad (15)$$

The basis (6) formed of products of Lagrange functions is strictly equivalent to a basis involving products of Laguerre polynomials

$$\begin{aligned} \tilde{F}_{ijk}^K(x, y, z) &\propto \mathcal{R}_K(x, y, z) L_i(x/h_x) L_j(y/h_y) \\ &\quad \times L_k(z/h_z) e^{-x/2h_x} e^{-y/2h_y} e^{-z/2h_z} \end{aligned} \quad (16)$$

with $i \in \{0, \dots, N_x - 1\}$, $j \in \{0, \dots, N_y - 1\}$, $k \in \{0, \dots, N_z - 1\}$, as employed, e.g., in Ref. [40]. The Lagrange-mesh calculation is thus equivalent to a variational calculation performed with basis (16) where the matrix elements would be calculated with the same Gauss-Laguerre quadrature. It has, however, a number of significant advantages over such a calculation. The potential matrix elements are very simple

with property (11), the Hamiltonian matrix is rather sparse, and this matrix is better conditioned.

For studying resonances, the Lagrange-mesh method can be combined [34] with the complex scaling method [35,36]. The coordinates x, y, z are then replaced by $e^{i\theta}x, e^{i\theta}y, e^{i\theta}z$, respectively, and Eq. (13) becomes

$$\sum_{Kijk} \left\{ e^{-2i\theta} \langle F_{i'j'k'}^{K'} | T_{K'K}^L | F_{ijk}^K \rangle_G + [e^{-i\theta} V(h_x u_i, h_y v_j, h_z w_k) - E(\theta)] \delta_{KK'} \delta_{i'i'} \delta_{j'j'} \delta_{kk'} \right\} C_{Kijk}^L(\theta) = 0. \quad (17)$$

The complex-scaled Hamiltonian matrix has the same sparse structure as the unscaled one and is symmetric but not Hermitian. For large enough values of θ smaller than $\frac{1}{2}\pi$, a resonant state corresponds to a square-integrable solution of the complex-scaled Schrödinger equation. The stationary values θ_0 of $E(\theta)$ with respect to θ in Eq. (17) provide approximations of the energy E_r and width Γ of the resonances as

$$E(\theta_0) = E_r - \frac{1}{2}i\Gamma. \quad (18)$$

III. ENERGIES, WIDTHS, AND MEAN DISTANCES

A. Conditions of the numerical calculations

When $\bar{p}\text{He}^+$ is considered as a three-body Coulomb system, all states of the antiprotonic helium atom are unstable except for the ground state and its electronic excited states. The first step of their search consists in looking for regions of the parameter space where the energies present plateaus of stationarity. Lagrange-mesh calculations depend on six parameters: three numbers of mesh points N_x, N_y, N_z and three scale parameters h_x, h_y, h_z . For low total angular momenta L , the shape of the system is very similar to a hydrogen atom with the He^{2+} nucleus and the antiproton very close to each other with respect to the electron mean distance [26,34]. The mean values of the perimetric coordinates x and y should then be very close to each other. Hence the choice $N = N_x = N_y$ and $h = h_x = h_y$ is a natural way of reducing the parameter space. We thus start with four free parameters and consider increasing L values.

Given that almost all states are unstable, the number of significant digits for the different observables is limited. Our strategy is thus to minimize the number of mesh points consistently with the accuracy achievable for each energy. In other words, after finding a stationary energy for some set of parameters, we try to reduce N and N_z without losing the accuracy on the significant figures.

A difficulty may occur by the fact that the lowest eigenvalues of the Lagrange-mesh matrix may represent unphysical square-integrable approximations of scattering states as well as square integrable approximations of physical resonant states. The mean values of the distances between the particles provide an easy way to discriminate physical and unphysical eigenvalues. This is also possible with the K probabilities discussed later. It may happen, however, that an unphysical energy is very close to a physical one and affects the accuracy of the calculation. When this problem occurs, it is usually easily solved by slightly increasing N or N_z .

TABLE I. Optimal parameters for $K_{\max} = L$ if $L = 0$ or 1 and $K_{\max} = 2$ if $L \geq 2$.

L	N	N_z	h	h_z	L	N	N_z	h	h_z	L	N	N_z	h	h_z
0	12	20	0.0003	0.38	17	14	12	0.0075	0.36	34	24	16	0.020	0.40
1	12	16	0.0007	0.44	18	14	12	0.0080	0.40	35	24	16	0.020	0.40
2	12	16	0.0010	0.34	19	14	12	0.0085	0.30	36	24	16	0.022	0.40
3	12	16	0.0014	0.36	20	14	12	0.0092	0.34	37	24	16	0.024	0.40
4	12	16	0.0016	0.34	21	16	12	0.0095	0.40	38	24	16	0.026	0.40
5	12	16	0.0019	0.40	22	16	12	0.0102	0.26	39	24	16	0.028	0.40
6	12	16	0.0024	0.40	23	16	12	0.0106	0.30	40	24	16	0.030	0.40
7	12	16	0.0028	0.40	24	16	12	0.0114	0.42	41	24	16	0.032	0.40
8	12	14	0.0034	0.40	25	16	12	0.0122	0.42	42	24	16	0.036	0.40
9	12	14	0.0040	0.36	26	16	12	0.015	0.36	43	26	14	0.040	0.40
10	12	14	0.0046	0.43	27	16	12	0.018	0.38	44	26	14	0.044	0.40
11	12	14	0.0052	0.38	28	16	22	0.017	0.60	45	28	12	0.048	0.40
12	12	12	0.0056	0.46	29	18	16	0.016	0.42	46	28	12	0.052	0.40
13	14	12	0.0060	0.52	30	22	16	0.015	0.40	47	30	12	0.056	0.40
14	14	12	0.0063	0.46	31	24	16	0.017	0.40	48	30	12	0.059	0.40
15	14	12	0.0067	0.48	32	24	16	0.018	0.42	49	32	10	0.062	0.40
16	14	12	0.0070	0.42	33	24	16	0.020	0.40	50	32	10	0.064	0.40

The sum over the hypermomentum quantum number K in Eq. (4) is truncated at some small value K_{\max} . Calculations of stationary energies have been performed for truncations at $K_{\max} = 0, 1, 2$, and 3 . While using $K_{\max} = 1$ yields noticeably different results from the case $K_{\max} = 0$, there is in general little difference between $K_{\max} = 1$ and 2 and almost no difference between $K_{\max} = 2$ and 3 , as can be seen below. Therefore the optimization of the parameters has been performed with $K_{\max} = 2$. The corresponding parameters are displayed in Table I.

The values of N and N_z are rather stable up to $L = 27$. They start increasing beyond that L value. Surprisingly, the choice $N_x = N_y$ and $h_x = h_y$ remains an acceptable simplification up to about $L = 50$ as we shall see below. The value of h increases rather steadily with L , except in a region of structure change around $L = 27$. Notice that in most cases, the energies are almost insensitive to variations of h in an interval around the quoted value. The value of h_z scatters around 0.40 in most cases. For small values of N_z , the results are quite sensitive to h_z .

While exploring the parameter space to find the (roughly) optimal values presented in Table I can take a lot of time in some cases, reproducing our results with these values using a Lagrange-mesh code is quite fast. It takes from seconds for the smallest basis sizes to less than half an hour for the largest one with $K_{\max} = 3$ on a fast personal computer. The time-consuming part of the calculation consists in the determination of a few low eigenvalues of the Hamiltonian matrix when it is large. The evaluation of this matrix from Laguerre zeros and weights is fast. The eigenvalue calculations are performed with the software JADAMILU [41]. The physical eigenvalue is usually found among the three lowest ones. For $L \leq 5$ and $L \geq 35$, it is in general the lowest one.

B. Energies as real stationary eigenvalues

The real stationary energies obtained for $L = 0-50$ and $K_{\max} = 0-3$ are gathered in Table II. Before discussing them

in more detail in Sec. IV, let us first make some general comments. The number of stable digits strongly varies with L . It decreases from $L = 0$ to $L = 23$ and increases beyond that value. Energies obtained with $K_{\max} = 0$ display a larger number of stable digits. They may be stationary for values of h_z different from those in Table I. The $K_{\max} > 0$ energies are obtained with the parameters of Table I. For $L \geq 3$, increasing K_{\max} from 0 to 1 reduces the number of stable digits and modifies the energies by an amount comprised between about 10^{-6} and 4×10^{-3} in the region $L = 20-30$. Changes are far less important for higher K_{\max} .

It should be noted that for unstable states, there may exist several local minima in the parameter space. In such cases, we have tried to choose the one which offered the weakest variation with the parameters. One can assume that the corresponding variation of several units on the last digit is roughly indicative of the width of the state. This assumption is analyzed in the next subsection.

The computer time increases with the product $N_x N_y N_z$. For high L values, it becomes interesting to reduce the number of mesh points by decoupling N_x from N_y and h_x from h_y . This is done for $L = 50, 60, 70$, and 80 in Table III. One observes that the same result is obtained for $L = 50$ with a reduction of $N_x N_y N_z$ by about 20% . Computer times are reduced at the cost of a more tedious exploration of the parameter space. With N_x almost constant and an increase of N_y , very accurate values can be obtained for the energies and mean radii.

C. Energies and widths from complex scaling

For a number of states for which few digits are stable, the complex scaling method has been used to compute resonance energies E_r and widths Γ . The FEAST software [42,43] has been used to compute the eigenvalues of the complex Hamiltonian matrix. The results are displayed in Table IV. The parameters h_x, h_y, h_z and the scaling angle θ are chosen to minimize the derivative of the energy with respect to θ . An accurate description of the square-integrable scaled resonance

TABLE II. Energies for $K_{\max} = 0 - 3$. All the displayed digits are stable with respect to variations of the numbers of points and scale parameters, except the last one, which may vary by a few units.

L	$K_{\max} = 0$	$K_{\max} = 1$	$K_{\max} = 2$	$K_{\max} = 3$
0	-2934.29714222503			
1	-733.94924619	-733.9492462		
2	-326.47742024	-326.477425	-326.477423	
3	-183.8622991	-183.862303	-183.862303	-183.862303
4	-117.8519093	-117.851910	-117.851910	-117.851910
5	-81.99447987	-81.99445	-81.99445	-81.99445
6	-60.373685186	-60.37364	-60.37364	-60.37364
7	-46.341108318	-46.3411	-46.3411	-46.3411
8	-36.72062357	-36.7205	-36.7205	-36.7205
9	-29.83941049	-29.8391	-29.8391	-29.8391
10	-24.74841862	-24.7480	-24.7480	-24.7480
11	-20.87669828	-20.876	-20.876	-20.876
12	-17.8640600	-17.863	-17.863	-17.863
13	-15.474173	-15.473	-15.473	-15.473
14	-13.5467634	-13.546	-13.546	-13.546
15	-11.9700392	-11.967	-11.967	-11.967
16	-10.6640987	-10.662	-10.662	-10.662
17	-9.570614	-9.570	-9.570	-9.570
18	-8.646207	-8.645	-8.645	-8.645
19	-7.858077	-7.857	-7.857	-7.857
20	-7.181057	-7.180	-7.180	-7.180
21	-6.5955767	-6.594	-6.594	-6.594
22	-6.0862498	-6.090	-6.090	-6.090
23	-5.6408336	-5.642	-5.642	-5.642
24	-5.249498	-5.2593	-5.2596	-5.2596
25	-4.904281	-4.90965	-4.90952	-4.90952
26	-4.598683	-4.602409	-4.60246	-4.60246
27	-4.327349	-4.330244	-4.330238	-4.330238
28	-4.0858553	-4.0881753	-4.0881909	-4.0881916
29	-3.87050248	-3.87240687	-3.87240909	-3.87240911
30	-3.6781948980	-3.679773780	-3.679774782	-3.679774786
31	-3.50632021075	-3.5076344917	-3.5076350336	-3.5076350311
32	-3.35266369810	-3.35375754525	-3.35375786353	-3.35375786378
33	-3.21533649578	-3.21624403698	-3.21624423242	-3.21624423252
34	-3.09271792469	-3.09346677930	-3.09346690183	-3.09346690187
35	-2.98340755026	-2.98402087684	-2.98402095422	-2.98402095424
36	-2.88618460130	-2.88668234139	-2.88668239015	-2.88668239016
37	-2.79997262723	-2.80037228493	-2.80037231539	-2.80037231540
38	-2.72380763649	-2.72412477408	-2.72412479286	-2.72412479286
39	-2.656808383794	-2.657056931562	-2.657056942960	-2.657056942961
40	-2.598148207134	-2.598340641362	-2.598340648167	-2.598340648168
41	-2.547029189946	-2.547176608811	-2.547176612819	-2.547176612819
42	-2.502661588544	-2.502773709070	-2.502773711414	-2.502773711414
43	-2.464253686380	-2.464338795496	-2.464338796870	-2.464338796870
44	-2.431017243672	-2.431082156644	-2.431082157463	-2.431082157463
45	-2.402189028156	-2.402239115582	-2.402239116083	-2.402239116083
46	-2.377060921427	-2.377100238930	-2.377100239248	-2.377100239248
47	-2.355006325327	-2.355037828728	-2.355037828939	-2.355037828939
48	-2.335493802411	-2.335519595495	-2.335519595641	-2.335519595641
49	-2.318086709779	-2.318108273733	-2.318108273838	-2.318108273838
50	-2.302433278998	-2.302451656877	-2.302451656956	-2.302451656956

states requires an increase of the numbers of mesh points with respect to Table I. The values of $N_x = N_y = N_z$ up to 22 have been considered.

The resonance energies E_r confirm the validity of the estimated energies E from Table III. It is interesting to note

that the width can be somewhat larger than the order of magnitude estimated from the stability of the real eigenvalues E . The widths increase progressively with L .

The perimetric coordinate system does not seem suited to give accurate widths beyond $L = 21$. Another method such

TABLE III. High- L parameters and energies ($K_{\max} \geq 1$).

L	N_x	N_y	N_z	h_x	h_y	h_z	E
50	26	32	10	0.062	0.064	0.40	-2.302451656955
60	28	38	10	0.080	0.100	0.40	-2.200975494690
70	28	42	10	0.088	0.146	0.40	-2.146362258771
80	28	50	10	0.120	0.198	0.40	-2.111899337302

as the Gaussian expansion method used beyond $L = 28$ in Refs. [8,15] would probably give good results.

D. Mean distances between the particles

For unstable states, mean values can not be defined rigorously since the wave functions are not square integrable. However, we have square-integrable approximations of these wave functions which describe their internal part and neglect their oscillating asymptotic part. We have computed the mean values of the distances between the three particles using these approximate wave functions. It is in this sense that we discuss mean distances below.

In the Lagrange-mesh method, the calculation of mean values is very simple and often very accurate by using the associated Gauss quadrature [see Eq. (15)]. Once the eigenvalues and eigenvectors are obtained, the computation of the mean distances between the particles takes a negligible time. As for the eigenvalues, the number of significant digits is estimated from the stability with respect to variations of the numbers of mesh points and of the scale parameters. In Table V we have, however, limited the number of significant

TABLE IV. Resonance energies E_r and widths Γ from complex scaling ($K_{\max} \geq 1$) compared with stationary energies E for $L = 2 - 21$. All the displayed digits are stable with respect to variations of the numbers of points and scale parameters, except the last one, which may vary by one or two units.

L	E	E_r	Γ
2	-326.477424	-326.477423	$< 10^{-6}$
3	-183.862303	-183.862303	2×10^{-6}
4	-117.851910	-117.851909	8×10^{-6}
5	-81.99445	-81.994465	2.5×10^{-5}
6	-60.37364	-60.373637	6.1×10^{-5}
7	-46.3411	-46.341003	1.3×10^{-4}
8	-36.7205	-36.720433	2.3×10^{-4}
9	-29.8391	-29.839104	4.0×10^{-4}
10	-24.7480	-24.74797	6.3×10^{-4}
11	-20.876	-20.87608	9.6×10^{-4}
12	-17.863	-17.86326	1.4×10^{-3}
13	-15.473	-15.47318	1.9×10^{-3}
14	-13.546	-13.5456	2.6×10^{-3}
15	-11.967	-11.9687	3.4×10^{-3}
16	-10.662	-10.6626	4.3×10^{-3}
17	-9.570	-9.5691	5.4×10^{-3}
18	-8.645	-8.6448	6.5×10^{-3}
19	-7.857	-7.8568	7.8×10^{-3}
20	-7.180	-7.1800	9.2×10^{-3}
21	-6.594	-6.5951	1.1×10^{-2}

digits to a maximum of 10 to save space, except for $\langle r_{\alpha\bar{p}} \rangle$ at $L = 0$.

For some L values, the electron-helium and electron-antiproton distances are not stable at all. They steadily increase when h_z or N_z increases. On the contrary, the antiproton-helium distances remain rather stable. Hence, for $L = 22-24$, we do not display $\langle r_{\alpha e} \rangle$ and $\langle r_{\bar{p}e} \rangle$. For $L = 15-21$ and possibly 25, the displayed values are mostly indicative of the fact that resonances replace quasibound states.

IV. DISCUSSION

We now discuss the results as a function of L with emphasis on the various changes occurring along the rotational band.

A. $L = 0$

Considered as a three-body Coulomb system, the ground state is the only stable state of $\bar{p}\text{He}^+$. With rather small numbers of mesh points ($N_x N_y N_z = 2880$) and short computing times of the order of 1 s, we obtain the $L = 0$ energy with an absolute accuracy estimated as a few times 10^{-11} , i.e., a relative accuracy better than 10^{-14} . The mean distances in Table V have relative accuracies better than 10^{-12} for $\alpha\bar{p}$ and 10^{-8} for the other two.

The $\alpha\bar{p}$ mean distance differs from 1.5 times the corresponding Bohr radius $a_{\alpha\bar{p}} = (m_{\bar{p}} + m_{\alpha})/2m_{\bar{p}}m_{\alpha} \approx 0.00034085518967666$ by about 4×10^{-14} . The $\alpha\bar{p}$ subsystem is thus very close to its free counterpart. The other two mean distances differ from 1.5 times the pseudohydrogen Bohr radius $a_{(\alpha\bar{p})e} = (m_{\bar{p}} + m_{\alpha} + m_e)/(m_{\bar{p}} + m_{\alpha})m_e \approx 1.0001095236$ by less than 5×10^{-7} . They agree with the picture of a $1s$ electron orbiting a charge 1 with mass $m_{\bar{p}} + m_{\alpha}$. This confirms the atomic interpretation of the system.

The $L = 0$ state has first been studied with high accuracy in Ref. [26] by using a nonorthogonal basis of 400 exponentials of the relative coordinates between the particles with random choices for the nonlinear parameters. In Ref. [26] the energy is obtained with an absolute accuracy of 10^{-12} and the mean distances with absolute accuracies of 10^{-10} for $\alpha\bar{p}$ and 10^{-11} for the other two. The authors also present accurately computed values for many other properties.

In order to compare with Ref. [26], we briefly adopt the same masses in this paragraph. With the conditions of calculation in Table I, we agree at the level of 2×10^{-10} for the energy. For the distances, our accuracy is significantly better for $\alpha\bar{p}$ and far less good for the other two. In order to deepen the comparison, we have tried to improve the agreement for the αe and $\bar{p}e$ mean distances. With $N = 16$, $h = 0.0003$, and $N_z = 55$, $h_z = 0.28$, our energy is still lower by 2×10^{-10} than in Ref. [26], but the αe and $\bar{p}e$ mean distances now agree at the level of accuracy of Ref. [26], i.e., about 10^{-11} , and the same for the $\alpha\bar{p}$ mean distances, i.e., at about 10^{-10} .

The $\bar{p}\text{He}^+$ ground state has also been studied in Ref. [44] within the Born-Oppenheimer approximation. In that work, the electronic energy curve is computed variationally and used as the electronic potential to determine the ground-state energy. With the same masses as in Ref. [44], the absolute

TABLE V. Mean distances between the particles as a function of L .

L	$\langle r_{\alpha\bar{p}} \rangle$	$\langle r_{\alpha e} \rangle$	$\langle r_{\bar{p}e} \rangle$	L	$\langle r_{\alpha\bar{p}} \rangle$	$\langle r_{\alpha e} \rangle$	$\langle r_{\bar{p}e} \rangle$
0	0.0005112827845555	1.50016385	1.50016392	27	0.27781	1.3221	1.4010
1	0.0017042759548	1.5001590	1.5001597	28	0.29943	1.3028	1.3908
2	0.003578984	1.500134	1.500144	29	0.3223988	1.264163	1.362456
3	0.0061354015	1.500074	1.500093	30	0.346655076	1.2364056	1.3467724
4	0.0093735426	1.49995	1.49999	31	0.372444330	1.2082960	1.3323751
5	0.01329341	1.49976	1.49984	32	0.3999745610	1.179592351	1.319125665
6	0.01789503	1.4994	1.4995	33	0.4294966122	1.150265153	1.307160231
7	0.0231784	1.4986	1.4989	34	0.4613152556	1.1203737598	1.2967599608
8	0.0291437	1.4978	1.4982	35	0.4958003099	1.0900358595	1.2883249922
9	0.0357905	1.4969	1.4974	36	0.5333974859	1.0594176072	1.2823726838
10	0.043119	1.4952	1.4959	37	0.5746361641	1.0287353012	1.2795475976
11	0.051126	1.495	1.496	38	0.6201281372	0.9982636565	1.2806331625
12	0.05982	1.491	1.493	39	0.6705464298	0.9683472642	1.2865528324
13	0.06918	1.494	1.496	40	0.7265677950	0.9394094299	1.2983411250
14	0.07925	1.490	1.493	41	0.7887617259	0.9119475301	1.3170575124
15	0.0899	1.51	1.51	42	0.8574247298	0.8864993332	1.3436213531
16	0.1014	1.50	1.50	43	0.9324023194	0.8635689240	1.3785834780
17	0.1135	1.49	1.50	44	1.0129950446	0.8435235931	1.4219197584
18	0.1263	1.51	1.52	45	1.0980434262	0.8265058260	1.4729749078
19	0.1399	1.49	1.50	46	1.1861837882	0.8124114709	1.5306191136
20	0.1541	1.52	1.53	47	1.2761436991	0.8009451603	1.5935366300
21	0.1688	1.62	1.64	48	1.3669363774	0.7917145575	1.6604924024
22	0.185			49	1.4579120899	0.7843149386	1.7304814344
23	0.201			50	1.5487120955	0.7783806293	1.8027629443
24	0.216			60	2.4503942977	0.7555957660	2.5965361818
25	0.2373	1.425	1.492	70	3.406359500	0.7515800365	3.503938357
26	0.25714	1.362	1.434	80	4.4694343806	0.7505906336	4.539745916

accuracy of the $\bar{p}\text{He}^+$ energy at the Born-Oppenheimer approximation is found as about 5×10^{-5} .

It is also instructive to use our accurate energy to test two other approximations of the energy based on the simple above picture which explained the values of some mean distances. If one neglects the distance between α and \bar{p} for the electron motion, the energy becomes the sum of the energy of the lowest state with orbital momentum L of the $\bar{p}\text{He}^{2+}$ hydrogenic ion and the energy of the $1s$ ground state of an hydrogenic atom with a nucleus of charge $Z = 1$ and mass $m_{\bar{p}} + m_{\alpha}$ [34]:

$$E_{\text{low } L} = -\frac{2m_{\alpha}m_{\bar{p}}}{(L+1)^2(m_{\alpha} + m_{\bar{p}})} - \frac{(m_{\alpha} + m_{\bar{p}})m_e}{2(m_{\alpha} + m_{\bar{p}} + m_e)}. \quad (19)$$

Another approximation can be obtained with a simple variational calculation using the product of a $1s$ He^+ wave function and an $(n = L + 1, L)\bar{p}\text{He}^{2+}$ wave function, both with adjustable effective charges determined by minimizing the energy [3]. This wave function in He^{2+} centered coordinates should give good results when an atomic structure dominates and provide a poor description of a molecular structure. The errors on both approximations for $L = 0$ amount to about 10^{-7} for the analytical approximation (19) and to about 10^{-5} for the variational calculation. These errors will also be discussed below for other L values and are displayed in Fig. 1.

B. $L = 1$

The $L = 1$ excited state may autoionize into an electron and an $\alpha\bar{p}$ hydrogenlike ion in its $L_{\alpha\bar{p}} = 0$ ground state with

energy -2933.79719683 . In spite of the large energy available for the emitted electron, this state is quasibound because of a width with an order of magnitude below 10^{-8} . The reason of this smallness of the width is the small overlap of the $\alpha\bar{p}$ parts of the initial $L = 1$ wave function and of the final wave function describing the electron emission. For $L_{\alpha\bar{p}} = 0$, the $\alpha\bar{p}$ mean distance is 5.11×10^{-4} and its root-mean-square deviation is 2.95×10^{-4} , while, for the $L = 1$ part of the $\alpha\bar{p}e$ system, they are 1.70×10^{-3} and 7.62×10^{-4} , respectively.

The αe and $\bar{p}e$ mean distances are slightly smaller than for $L = 0$.

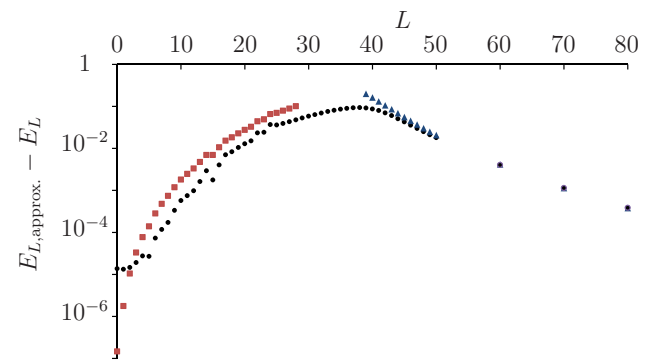


FIG. 1. Accuracies of approximate energies $E_{L,\text{approx}}$ in a.u. for the low- L analytical approximation (19) (red squares), variational approximation (black dots), and high- L analytical approximation (22) (blue triangles).

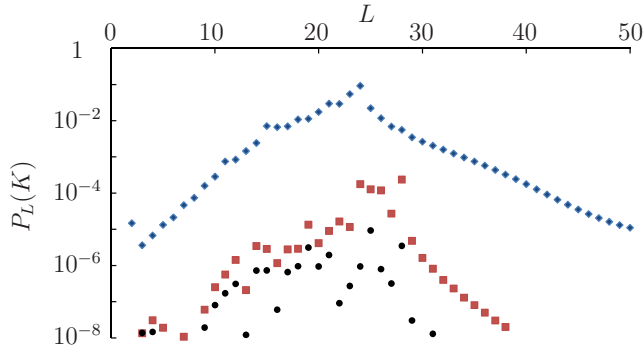


FIG. 2. Probabilities $P_L(K) = \sum_{ijk} (C_{kijk}^L)^2$ of the $K = 1$ (blue diamonds), $K = 2$ (red squares), and $K = 3$ (black dots) components.

C. $L = 2-14$

The $L = 2$ state can decay to $L_{\alpha\bar{p}} = 1$ and 0. The search for a stationary energy for this state was difficult because several local plateaus occur. This state seems to correspond to a first shape transition although it is not easy to characterize it. One observes that, contrary to $L = 1$ where the intrinsic state is essentially purely rotational with a $K = 1$ probability smaller than 10^{-9} , the $L = 2$ state has a small but significant $K = 1$ component with a probability larger than 10^{-5} as shown in Fig. 2. The $K = 2$ component is negligible. Nevertheless, the absolute uncertainty on the energy is around 10^{-6} , and the width was too small to be obtained with the present complex scaling method.

For $2 < L \leq 14$, the number of stable digits of the energies progressively decreases. The $K = 1$ component increases, but higher- K components remain essentially negligible and the stable results with $K_{\max} > 1$ are identical to those with $K_{\max} = 1$. The accuracy on the energies confirms that the states can still be considered as quasibound. This is confirmed by the complex scaling calculations. The widths increase from 2×10^{-6} for $L = 3$ to 2.6×10^{-3} for $L = 14$. With respect to the resonance energies E_r , the stationary energies E have an accuracy better than 10^{-3} .

From $L = 3$, the variational approximation of the energies becomes better than the analytical formula (19). At $L = 14$, its absolute error is 3×10^{-3} , i.e., a relative error of 2×10^{-4} .

For all these states, the αe and $\bar{p}e$ mean distances slightly decrease with L . The decrease is smaller than a percent at $L = 14$. The $\alpha\bar{p}$ mean distance is very close to the hydrogenlike expression for a state with $L = n - 1$,

$$\langle r \rangle_{\alpha\bar{p}} = \frac{1}{2}(L+1)(2L+3)a_{\alpha\bar{p}} \approx 0.000170(L+1)(2L+3), \quad (20)$$

as shown in Fig. 3.

D. $L = 15-21$

At $L = 15$, the number of stable digits remains quite large for $K_{\max} = 0$ but, for $K_{\max} > 0$, the last digit of the stationary value, displayed in Table II, becomes less stable, and its determination by this method is less accurate. The energy

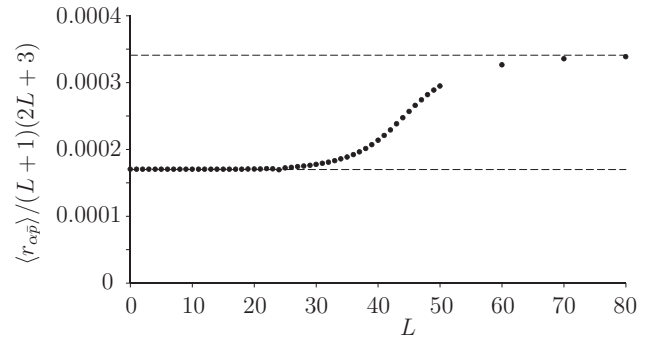


FIG. 3. $\langle r_{\alpha\bar{p}} \rangle$ mean distances in a.u. divided by $(L+1)(2L+3)$ as a function of L . The dotted lines correspond to the low- L [Eq. (20)] and high- L [Eq. (21)] limits.

at the middle of the small stationary plateau is nevertheless consistent with the resonance energy (see Table IV). Also, the accuracy on the mean distances drops significantly. The $K = 1$ component strongly increases. The width of the resonance and the $\alpha\bar{p}$ mean distance, however, do not show any irregularity in their steady increase.

From $L = 15$ to $L = 21$, the resonances become wider and the mean distances less stable. The $K = 1$ component reaches 3%, and the $K = 2$ one increases. The fluctuations of the $K = 3$ probabilities are probably due to the difficulty of locating the optimal value for the h_z scale parameter. On the contrary, the results are quite insensitive to the precise value of h .

Since the values of $\langle r_{\alpha\bar{p}} \rangle$ remain rather accurate and much smaller than the other two, one can still interpret these narrow resonances as states of a hydrogen pseudoatom. This is confirmed both by the L dependence of $\langle r_{\alpha\bar{p}} \rangle$ in Fig. 3 and by the good variational approximation on the energy in Fig. 1. This remains true up to about $L = 25$, but an important change occurs at $L = 22$.

E. $L = 22-27$

Up to now, all excited states are in principle able to decay toward all lower states. Nevertheless, transitions where the electron carries the smallest orbital momentum l are favored if the corresponding emitted energy is large enough. For given $L \leq 21$, the closest open channel corresponds to $L_{\alpha\bar{p}} = L - 1$, and the electron can carry an angular momentum $l = 1$.

The situation changes at $L = 22$: the channel $L_{\alpha\bar{p}} = 21$ is closed, and the dominant transition leads to $L_{\alpha\bar{p}} = L - 2$ with $l = 2$. The energy gap increases from 0.06 for $L = 21$ to 0.56 for $L = 22$ (see Fig. 4). This implies that the width variation might not be large despite the change of l value.

In the range $L = 22-27$, a number of changes occur. The search for stationary energies becomes uncertain. As shown by Table I, irregularities appear in the determination of h and h_z . The $\langle r_{\alpha e} \rangle$ and $\langle r_{\bar{p}e} \rangle$ mean values cannot be determined for $L = 22-24$. They are too sensitive to the uncertain h_z but are again rather stable at and beyond $L = 25$ where they start decreasing. While Fig. 3 shows that the value of $\langle r_{\alpha\bar{p}} \rangle$ still follows expression (20), small fluctuations appear. The $K = 1$

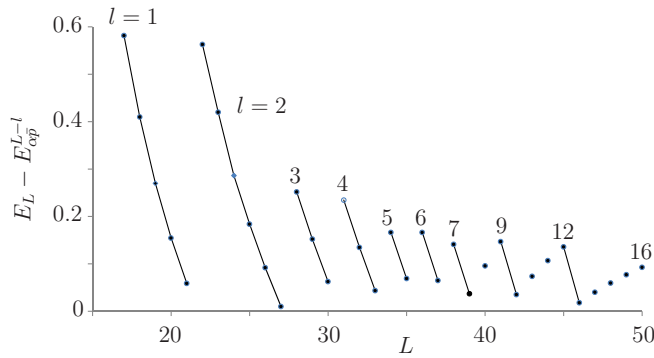


FIG. 4. Electron emission energy in a.u. for the lowest orbital momentum l as a function of L , where $E_{\alpha\bar{p}}^{L-l}$ is the energy of the highest open threshold with $L_{\alpha\bar{p}} = L - l$.

probability reaches a maximum of 10% at $L = 24$, and the other probabilities also reach their maxima around $L = 25$.

All this indicates the start of a structure change. The widths of the resonances must reach their maximum and then begin to decrease. The hydrogen pseudoatom description ceases to be valid as well as the analytical approximation (19) as shown by Fig. 1. The simple atomic variational approximation gets poorer and poorer. At $L = 27$, the threshold energy for the emission of an $l = 2$ electron almost vanishes (see Fig. 4).

F. $L = 28-42$

At $L = 28$, the $L_{\alpha\bar{p}} = 26$ threshold is closed, and the most favorable spontaneous emission of an electron requires $l = 3$ (see Fig. 4). For this reason probably, at this L value, it was extremely difficult to find optimal conditions for the calculation. Among various local minima, the lowest one presented here is quite special with an unusually large number N_z of mesh points and a very large h_z .

Beyond $L = 28$, a higher number of stable digits can be reached since the widths become very small [8]. To this end, N is progressively increased to 24 while N_z is chosen as 16. The h value becomes proportional to $\langle r_{\alpha\bar{p}} \rangle$, and the h_z value

stabilizes at 0.40. The optimization in this region is easy: N , N_z , and h_z are constant, and h regularly increases. One observes that h is roughly equal to $0.042\langle r_{\alpha\bar{p}} \rangle$. Ten digits of the energy are stable even for the $K_{\max} = 1$ approximation, which is excellent. The probability of the $K = 1$ component decreases exponentially.

The energy slowly increases with L . As the angular momentum carried out by the electron increases from $l = 3$ to $l = 9$, the stationary value of the energy becomes a local minimum and the states more and more resemble bound states.

In this whole range, the system keeps its moleculelike structure with various shapes. The mean distances vary in different ways. In Fig. 3 the $\langle r_{\alpha\bar{p}} \rangle$ mean value starts to deviate from the low- L limit by increasing faster than in expression (20). On the contrary, $\langle r_{\alpha e} \rangle$ steadily decreases and $\langle r_{\bar{p}e} \rangle$ passes through a minimum at $L = 37$, the former becoming significantly smaller than the latter. The system has turned to a moleculelike structure with, however, the important difference that the heavy particles repel each other. This is confirmed by the poor quality of the results with the simple atomic variational wave function.

In this L range, accurate results from Ref. [14] (as updated in Table 26 of Ref. [1]) and from Ref. [8] are available. They allow a comparison of the energies and an external test of their accuracies (see Table VI). The variational basis in Ref. [14] involves bipolar harmonics and exponentials in atomic coordinates with respect to He^{2+} . In Ref. [8] an expansion in bipolar harmonics and Gaussians combining the three sets of Jacobi coordinates is employed. For $L = 28$, our $K_{\max} = 3$ value agrees within better than 10^{-6} with Ref. [8]. As the width is 2.8×10^{-7} [8], our stationary value could not be much more precise especially with the complicate structure of this transition state. The accuracy improves fast beyond that value. For $L = 29$, the agreement reaches 2×10^{-8} for a width of 3.5×10^{-8} . Beyond $L = 30$, the width is smaller than 10^{-9} [8]. This can be understood by the fact that the electron must carry out an orbital momentum $l = 4$ from $L = 31$ and $l = 5$ from $L = 34$. The states are again quasibound.

TABLE VI. Comparison with non relativistic results of Kino *et al.* [8] and of Korobov [14] as updated in Ref. [1]. The energies E are taken from Table II, and the energies E' are calculated with the masses $m_\alpha = 7294.299$ and $m_{\bar{p}} = 1836.1527$ of Ref. [14].

L	E	Kino <i>et al.</i>	E'	Korobov
28	-4.0881916	-4.088190936		
29	-3.87240911	-3.872409094		
30	-3.679774786	-3.679774778	-3.679774782	-3.6797747922
31	-3.5076350311	-3.507635035	-3.5076350339	-3.5076350346
32	-3.35375786378	-3.353757863	-3.35375786388	-3.3537578640
33	-3.21624423252	-3.216244231	-3.21624423274	-3.2162442328
34	-3.09346690187	-3.093466899	-3.09346690211	-3.0934669021
35	-2.98402095424	-2.984020954	-2.98402095448	-2.9840209545
36	-2.88668239016	-2.886682386	-2.88668239038	-2.8866823904
37			-2.80037231560	-2.8003723156
38			-2.72412479305	-2.7241247931
39			-2.657056943126	-2.6570569431
40			-2.598340648313	-2.5983406483
41			-2.547176612946	-2.5471766129

At $L = 30$ and 31 , Korobov's energies are lower than ours and thus probably a little better. Beyond $L = 33$, our accuracy reaches 10^{-11} . Our values are a little below the results of Ref. [8] and agree perfectly with those of Korobov.

G. $L \geq 43$

At $L = 43$, $\langle r_{\alpha e} \rangle$ becomes smaller than $\langle r_{\alpha \bar{p}} \rangle$, and the system enters in another regime. To keep a good accuracy, N must slowly increase while N_z can slowly decrease.

The new geometry of the system now resembles a pseudoatom, but a different one. The antiproton surrounds a diffuse He^+ core with a radius a little larger than the mean radius of a free He^+ ion. This pseudoatom possesses an infinity of quasibound states. Its highly excited states are Rydberg-like states. The energy tends to the asymptotic He^+ value $-2m_\alpha m_e / (m_\alpha + m_e)$. The $\langle r_{\alpha \bar{p}} \rangle$ mean distance tends to its asymptotic value

$$\begin{aligned} \langle r \rangle_{\text{He}^+ \bar{p}} &= \frac{1}{2}(L+1)(2L+3)a_{\text{He}^+ \bar{p}} \\ &\approx 0.000341(L+1)(2L+3), \end{aligned} \quad (21)$$

with $a_{\text{He}^+ \bar{p}} = (m_\alpha + m_{\bar{p}} + m_e) / (m_\alpha + m_e)m_{\bar{p}}$. This high- L limit is about twice the low- L value in Eq. (20). This trend is already visible in Fig. 3. At $L = 80$, $\langle r_{\alpha \bar{p}} \rangle / (81 \times 163)$ is equal to 0.0003385.

Around $L = 50$, it becomes more economical to decouple N_x , h_x from N_y , h_y (see Table III). Of course, the search for optimal parameters has become more tedious, but calculations are faster than with $N_x = N_y$ when they are selected. Energies can be obtained with 12 significant digits when N_y is large enough.

The variational approximation starts to improve at $L = 39$. It tends to a high- L analytical approximation involving the He^+ energy and the $(n = L + 1, L)$ hydrogenlike energy of an antiproton orbiting a He^+ core,

$$E_{\text{high } L} = -\frac{2m_\alpha m_e}{m_\alpha + m_e} - \frac{(m_\alpha + m_e)m_{\bar{p}}}{2(L+1)^2(m_\alpha + m_{\bar{p}} + m_e)}, \quad (22)$$

with a relative accuracy of about 1.5% at $L = 48$. At $L = 80$, the accuracy of expression (22) and of the variational approx-

imation is 4×10^{-4} . The error seems to decrease roughly as $\exp(-L/10)$.

V. CONCLUSION

In previous works, the antiprotonic helium atom was mostly studied around total orbital momentum $L = 35$, through which the antiproton mass is most accurately determined until now. This system, however, presents an interesting variety of structures across a wide range of L values, which deserves to be studied. In this paper, we analyze the evolution of the system structure with L by focusing on the states with the lowest electronic excitation. These states are characterized by a strongly dominant $K = 0$ component along the $\alpha \bar{p}$ axis and define what we refer to as the lowest rotational band. Among them, only the ground state is stable, while the others are resonances with various degrees of instability.

From $L = 0$ up to $L \approx 25$ along its lowest rotational band, the system behaves as a pseudoatom with a progressively expanding He^{2+} nucleus + antiproton core. Along this evolution, the width for the spontaneous emission of the electron increases from smaller than 10^{-8} up to at least 10^{-2} . Around $L = 27$, a transition occurs to a moleculelike structure. The width then decreases and becomes again smaller than 10^{-8} above $L = 30$. This is due to a fast increase of the orbital momentum carried out by the emitted electron. Above $L = 42$, a new transition occurs to a pseudoatom structure with the antiproton orbiting a He^+ core. An infinity of such states exist with, progressively, a Rydberg-atomlike structure. The electron emission width becomes so small that these states can be considered as belonging to a stable Coulomb system. The main deexcitation channel comes from photon emission [1].

The numerical study of this system is very efficient with the Lagrange-mesh method after a sometimes tedious search for four or six optimized parameters. With these parameters, our results can easily be reproduced with rather short computation times. Wave functions are available in a practical form allowing a simple evaluation of observables with the Gauss quadrature associated with the three-dimensional mesh. The Lagrange-mesh method, or probably the need to use perimeteric coordinates to avoid problems with the singularities of the Coulomb potentials, is less efficient for rather broad resonances when combined with the complex-scaling method. Another approach would be necessary in the $L \geq 22$ domain.

[1] T. Yamazaki, N. Morita, R. S. Hayano, E. Widmann, and J. Eades, *Phys. Rep.* **366**, 183 (2002).
 [2] G. T. Condo, *Phys. Lett.* **9**, 65 (1964).
 [3] J. E. Russell, *Phys. Rev. A* **1**, 721 (1970).
 [4] J. E. Russell, *Phys. Rev. A* **1**, 735 (1970).
 [5] J. E. Russell, *Phys. Rev. A* **1**, 742 (1970).
 [6] M. Iwasaki, S. N. Nakamura, K. Shigaki, Y. Shimizu, H. Tamura, T. Ishikawa, R. S. Hayano, E. Takada, E. Widmann, H. Outa, M. Aoki, P. Kitching, and T. Yamazaki, *Phys. Rev. Lett.* **67**, 1246 (1991).
 [7] V. Korobov, *Nucl. Phys. A* **689**, 75 (2001).

[8] Y. Kino, H. Kudo, and M. Kamimura, *Mod. Phys. Lett. A* **18**, 388 (2003).
 [9] S. I. Fedotov, O. I. Kartavtsev, and D. E. Monakhov, *Yad. Fiz.* **59**, 1717 (1996) [*Phys. Atom. Nucl.* **59**, 1662 (1996)].
 [10] V. I. Korobov, *Phys. Rev. A* **54**, R1749 (1996).
 [11] V. I. Korobov and D. D. Bakalov, *Phys. Rev. Lett.* **79**, 3379 (1997).
 [12] N. Elander and E. Yarevsky, *Phys. Rev. A* **56**, 1855 (1997).
 [13] Y. Kino, M. Kamimura, and H. Kudo, *Nucl. Phys. A* **631**, 649 (1998).

- [14] V. I. Korobov, D. Bakalov, and H. J. Monkhorst, *Phys. Rev. A* **59**, R919 (1999).
- [15] Y. Kino, M. Kamimura, and H. Kudo, *Nucl. Instrum. Methods Phys. Res., Sec. B* **214**, 84 (2004).
- [16] M. Hesse and D. Baye, in *Few-Body Problems in Physics*, edited by N. Kalantar-Nayestakani, R. G. E. Timmermans, and B. L. G. Bakker, AIP Conference Proceedings Vol. 768 (American Institute of Physics, New York, 2005), pp. 328–330.
- [17] Y. Kino, M. Kamimura, and H. Kudo, *Hyperfine Interact.* **119**, 201 (1999).
- [18] V. I. Korobov, L. Hilico, and J.-P. Karr, *Phys. Rev. A* **89**, 032511 (2014).
- [19] V. I. Korobov, L. Hilico, and J.-P. Karr, *Hyperfine Interact.* **233**, 75 (2015).
- [20] V. I. Korobov and I. Shimamura, *Phys. Rev. A* **56**, 4587 (1997).
- [21] J. Révai and A. T. Kruppa, *Phys. Rev. A* **57**, 174 (1998).
- [22] T. Yamazaki and K. Ohtsuki, *Phys. Rev. A* **45**, 7782 (1992).
- [23] I. Shimamura, *Phys. Rev. A* **46**, 3776 (1992).
- [24] M. Hori, A. Dax, J. Eades, K. Gomikawa, R. S. Hayano, N. Ono, W. Pirkel, E. Widmann, H. A. Torii, B. Juhász, D. Barna, and D. Horváth, *Phys. Rev. Lett.* **96**, 243401 (2006).
- [25] M. Hori, H. Aghai-Khozani, A. Sótér, D. Barna, A. Dax, R. Hayano, T. Kobayashi, Y. Murakami, K. Todoroki, H. Yamada, D. Horváth, and L. Venturelli, *Science* **354**, 610 (2016).
- [26] V. H. Smith Jr. and A. M. Frolov, *J. Phys. B* **28**, 1357 (1995).
- [27] A. S. Coolidge and H. M. James, *Phys. Rev.* **51**, 855 (1937).
- [28] C. L. Pekeris, *Phys. Rev.* **112**, 1649 (1958).
- [29] D. Baye and P.-H. Heenen, *J. Phys. A* **19**, 2041 (1986).
- [30] M. Vincke, L. Malegat, and D. Baye, *J. Phys. B* **26**, 811 (1993).
- [31] D. Baye, M. Hesse, and M. Vincke, *Phys. Rev. E* **65**, 026701 (2002).
- [32] M. Hesse and D. Baye, *J. Phys. B* **32**, 5605 (1999).
- [33] M. Hesse and D. Baye, *J. Phys. B* **36**, 139 (2003).
- [34] D. Baye, *Phys. Rep.* **565**, 1 (2015).
- [35] J. Nuttall and H. L. Cohen, *Phys. Rev.* **188**, 1542 (1969).
- [36] Y. Ho, *Phys. Rep.* **99**, 1 (1983).
- [37] M. Hesse and D. Baye, *J. Phys. B* **34**, 1425 (2001).
- [38] Z. Zhen, *Phys. Rev. A* **41**, 87 (1990).
- [39] J. Dohet-Eraly, *Eur. Phys. J. Plus* **132**, 362 (2017).
- [40] B. Grémaud, D. Delande, and N. Billy, *J. Phys. B* **31**, 383 (1998).
- [41] M. Bollhöfer and Y. Notay, *Comput. Phys. Commun.* **177**, 951 (2007).
- [42] E. Polizzi, *Phys. Rev. B* **79**, 115112 (2009).
- [43] J. Kestyn, E. Polizzi, and P. T. P. Tang, [arXiv:1506.04463](https://arxiv.org/abs/1506.04463) (2015).
- [44] A. C. Todd and E. A. G. Armour, *J. Phys. B* **38**, 3367 (2005).